Investigation of Fluid Flow Through Varying Microfluidic Conditions

Divy Raval - November 27, 2019

Introduction

Microfluidics concerns itself with the motion of fluids through (micro) channels, where it has found engineering applications since the twentieth century in the industry, molecular biology, and more. The high-level objective of the investigation was to gain an understanding of the science of microfluidics by experimenting with the flow of a bead solution under varying geometries and conditions.

The analysis of the data relied on measuring the velocity V in m/s of the fluid using

$$V = \Delta s/\Delta t \qquad Velocity\ 1$$

where distance s is in SI units of meters, and time t is in SI units of seconds. The distance was obtained by measuring the pathline of the flowing beads, while the change in time was taken to be the exposure time of a given image. The results all came from the collected images generated by the laboratory software.

To begin understanding the behaviour of moving fluids, a Newtonian generalization is made which provides that the shear stress of an incompressible fluid is proportional to the velocity gradient:

$$\tau = \mu \frac{du}{dy} \qquad Shear\ Stress\ 2$$

The shear is theoretically greatest at near walls and slowly decreases as dy grows away from zero, this fact can be proven simply by plugging values into equation (2).

Experimental Procedure

The procedure from the laboratory manual [1] was followed without deviation. The channels on the microfluidic chip using in this investigation are referred to as channels 1 to 4 which contain an abrupt-transition, smooth-transition, abrupt-bends, and smooth-bends respectively. Their figures can be seen in the lab manual.

Results

All channels used through this investigation contained observable imperfections (as seen in Figure 1)[1]. Though these are likely to cause some amount of turbulence/non-laminar flow, they are not large relative to the channel to significantly disrupt flow further away from the walls.

From the lab manual, the provided-true measurements were utilized to generate a pixel per meter scale in ImageJ[2] [2] to determine displacements in meaningful (meters) units. Figure 2 shows a sample of screenshot of how the scaling occurred while adjacently Table 1 stores the scaling ratios. The appropriate scaling was used for the purposes of data analysis dependant on the objective of a given image.

A simple analysis was done to determine the effects of gravitational energy on the fluid, Table 2 summarizes the results which indicate a 14000% (errors to be discussed later) as the syringe elevation is increased from a low to relatively higher position.

Using equation (1) to calculate velocities of a fluid at a given position, Figure 3 (left) was plotted by fitting the data points of a straight channel with the gravity head volume at 2.5mL, 1.3mL, and 0.7mL. Then finding a similar trend among each fits displays a parabolic relationship between the velocity and relative distance from the wall. The quadratic regression and some

[1] Figures and tables are presented in the Appendix found at the very end of this report.

[2] ImageJ is the measurement software which was used to determine the displacement and position of a particle.

other functionalities/algorithms throughout this investigation were implemented using NumPy [2] - a scientific computing library. To determine a relationship between velocity and volume, the average velocity was plotted against the volume, where the average velocity was determined using the general average-function-value formula where a and b are the wall boundaries.

$$f_{avg} = \frac{1}{b-a}\int_a^b f(x)\ dx \qquad Average\ f(x)\ 3$$

The relationship is plotted in Figure 4 (left) and can be seen to have a positive correlation, as the volume increases, so does the velocity of the fluid. Repeating the velocity-volume experiment on channels with transitioning widths (Figure 4, right) also resulted in a positive correlation between velocity and volume.

The velocity of channels with varying widths was compared before and after the transitions for the gradual and abrupt transitions, both showed an increase in velocity after the flow went through the transitions, where the widths of the channels were smaller after the transition. The results are formatted in Table 3 and suggest an inverse proportionality between the flow and channel width. Looking at Figure 5 (left) and (middle), the gradual transition had pathlines with less curvature – more linearity, whereas the abrupt transition had noticeably more non-linear pathlines. The reading errors for all calculations are presented in Table 4.

Bends in a channel result in negligible effects to the mean velocity before and after the change in orientation, meanwhile with marginal increases to velocity in the bends (Table 5). There is laminar flow observed before and after the bends, but also inside the bends, with similar distributions observed when plotted as previously seen in Figure 3.

Error Analysis

The previously referenced Table 4 contains the fundamental reading errors/uncertainties of the syringe-volume, digital scale measurement, and the time elapsed taken to their lowest significant digit. To propagate these uncertainties the general, multivariable uncertainty formula was used when possible

$$\delta f = \sqrt{(|f_x|\delta f_x)^2 + \left(|f_y|\delta f_y\right)^2 + \ldots + (|f_i|\delta f_i)^2} \qquad Error\ 4$$

with δf is the uncertainty for some quantity $f(x, y, \ldots, i)$, and f_i represents the partial derivative of f with respect to the ith parameter.

Equation (4) was directly used on equation (1) to produce an uncertainty for the velocity, however, the uncertainty was a local error which assumed that the only uncertainties were produced from Table 4 which is not correct – hence the uncertainties were very small before the standard deviation of the data set was taken into consideration. The velocity uncertainties were on the order of magnitude of $\sim 1 - 10\%$, however by using computer programs to generate a distribution of the velocities, standard deviations were generated at a scale more representative to the sources of errors present in this investigation.

Though it is not easy to generate errors or chi-squared values on NumPy's quadratic regression algorithm, a residual plot (Figure 3, right) was generated using the following equation:

$$\varepsilon = X - \bar{X} \qquad Residual\ 5$$

The residual formula generates a point by subtracting the actual value and the fitted value, hence a smaller ε (closer to the horizontal line at 0) represents a better fit. Thus the quadratic

fits were not ideal and possed significant uncertainties. All of the uncertainties (standard deviations of the data) presented seem reasonable because most of the data overlap when the uncertainty ranges are considered.

Other uncertainties not accounted for throughout this investigation, but were definitely prominent was the idealization of orthogonality of images in the X and Y axis to determine the distance from the walls (hence the slightly skewed Figure 3 (left)), assuming that widths throughout the analysis remained consistent before and after a bend which is not factually correct, not considering the possibility of turbulent flow near the edges of the channel, and the largest was human error involved in selecting and measuring the sample points creates vast uncertainty. In the future, many of these uncertainties can be reduced or avoided by using better equipment, and technology to automatically track the velocity of particles at low exposures.

Discussion

In straight channels, the maximum velocity is expected to be seen at the location in between the two walls, while the largest difference is noticed at the walls because the shear force is greatest (in accordance with equation 2). Observing Figure 2 (left), the flow observed is laminar and aligns with the maximum velocity being central relative to the wall positions. The quadratics presented in the plot are fitted using quadratic regression, where their error is shown in the residual plot (Figure 2, right).

To increase or decrease the velocity profile, the plot in Figure 4 (left) indicates that increasing the volume of the fluid in the syringe correlates to a greater velocity, and Table 2 similarly shows that a greater gravitational potential energy relative to the chip results in increased velocity. In Figure 4 (left) plot, the fitted functions for velocity through equation (3) in order to generate an average value to plot the volume against.

Channels that change width through a transitional portion are shown to result in no changes in their laminar velocity, within the standard deviation, as shown in Table 3. The table additionally corroborates the fact that gravitational potential energy has the same effect on channels of different sizes as it does on straight channels. Table 3 says nothing about the velocity of the fluid in the bends, only before and after the width of the channel has changed due to the transition.

Looking at Figure 5 (left) and (middle) display a fluorescent view of the bead solution flowing through the channels. The gradual transition has more linear pathlines and the central, laminar flow effects can be seen to continue as there are some extended pathlines that continue directly through the transition into the smaller width. In contrast, the channel with abrupt change has less smooth flow, especially at the walls where the shear force is greatest. The abrupt transition leaves open a greater possibility for turbulence in the condition of irregular flow patterns whereas this is not as noticeable in the gradual transition.

Channels 3 and 4 consisted of two-dimensional bends, similar to transitions of channels 1 and 2, except the width parameter is constant within some epsilon. Much like the results of width changes in a channel, the velocity profiles are consistent within the indicated standard deviation in Table 5 before and after the bends. However, both the sharp and smooth curve bends resulted in a small fractional increase in mean velocity – these can largely be associated with human errors and falling within the standard deviation.

Figure 5 (right) highlights the pathlines of particles around a curve with a thin white outline and demonstrates the difficulty of judging what defines a particle in a curve, and the accuracy to which it can be traced without software. By repeating the analysis process as in Figure 3, it was determined that the channels with bends also exhibited laminar flow.

Conclusion

Utilizing measurement software and scientific computing packages, data were analyzed to determine that the velocity profiles as seen in Figure 3 (left) are consistent with the shear force exhibited by idealized Newtonian fluids, where the velocity is lowest at the walls and peaks quadratically at a vertex located between the walls. By implementing error analysis, it was determined that the standard deviation for much of the data was fairly large due primarily to human error, however, within those uncertainties it was concluded using the data from Tables 2, 3, and 5 that laminar flow was exhibited throughout all channels with the exception of some small delta-distance away from the walls where there could have been turbulent flow through the observations in Figure 1 (right) under 40X objective.

Additionally, it was found that the volume in the syringe which the fluid is leaked from results in a positive relationship between the volume and average velocity (Figure 4). Additionally increasing the highest relative to the chip reference height also exhibited a positive correlation. Thus it agrees with general concepts of physics where greater potential energies (pressure and gravitational) must be conserved in a control volume system, hence the kinetic energy (and thereby the velocity) was some function of both of those along with other parameters of the channel such as width and curvature.

References

[1] B. Keith, E. Chung, and T. Dell, "Introduction to Microfluidics," *Quercus*. [Online]. Available: https://q.utoronto.ca/courses/119723/files/4201607?module_item_id=863360. [Accessed: 23-Nov-2019].

[2] W. Rasband, *ImageJ*. [Online]. Available: https://imagej.nih.gov/ij/index.html. [Accessed: 26-Nov-2019].

[3] *SciPy*. [Online]. Available: https://docs.scipy.org/doc/numpy/index.html. [Accessed: 25-Nov-2019].

Appendix: Figures and Tables

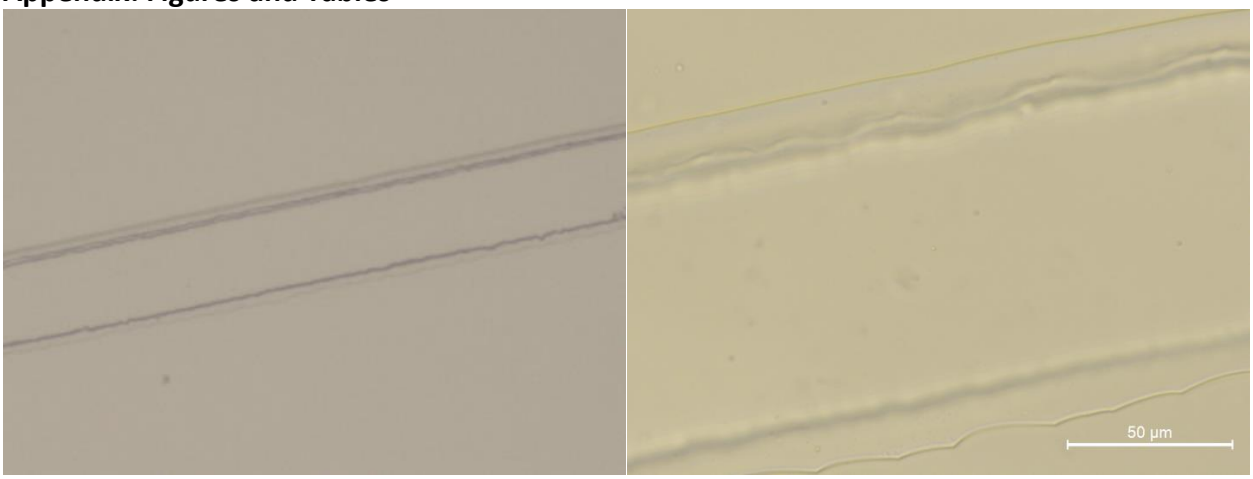

Figure 1: (left) 5X objective magnification on a straight portion of a channel. (right) 40X objective magnification on the same straight portion as (left) image.

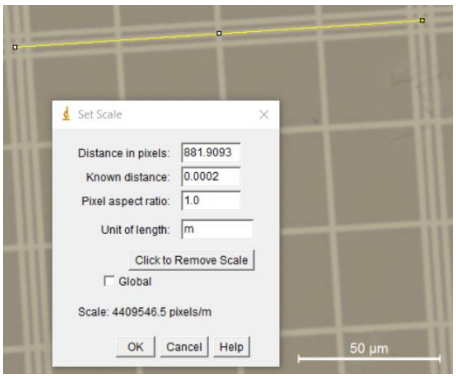

Figure 2: Software image used to determine the digital scaling ratio of the collect images.

Objective	*Hemocytometer Equivelent(m)*	*Digital Scaling Ratio (px/m)*
5X	0.001	546.3511/0.001
10X	0.0002	214.9315/0.0002
20X	0.0002	438.3160/0.0002
40X	0.0002	881.9093/0.0002

Table 1: Digital scaling ratios of images collected at 5X, 10X, 20X, and 40X objectives

Relative Elevation	*Mean Velocity (m/s)*	*Standard Deviation (%)*
Low	0.00073	±56
High	0.10	±42
% Increase	14000%	

Table 2: Comparing the velocity of fluid flow through a straight channel as the relative elevation of the syringe changes.

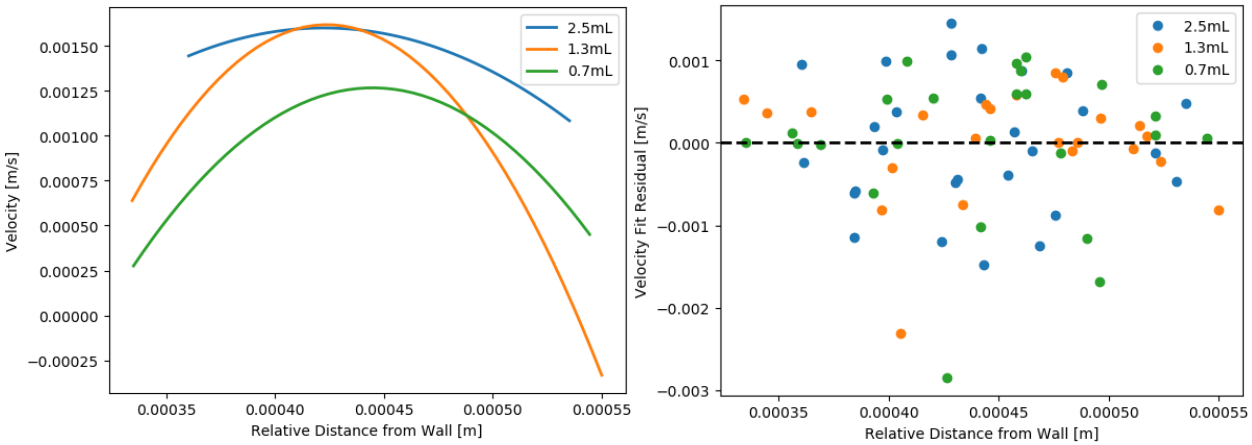

Figure 3: (left) Fitted velocities of three different volume-conditions - 2.5mL, 1.3mL, 0.7mL - of the flow through a straight channel. (right) Residuals of each volume condition fit.

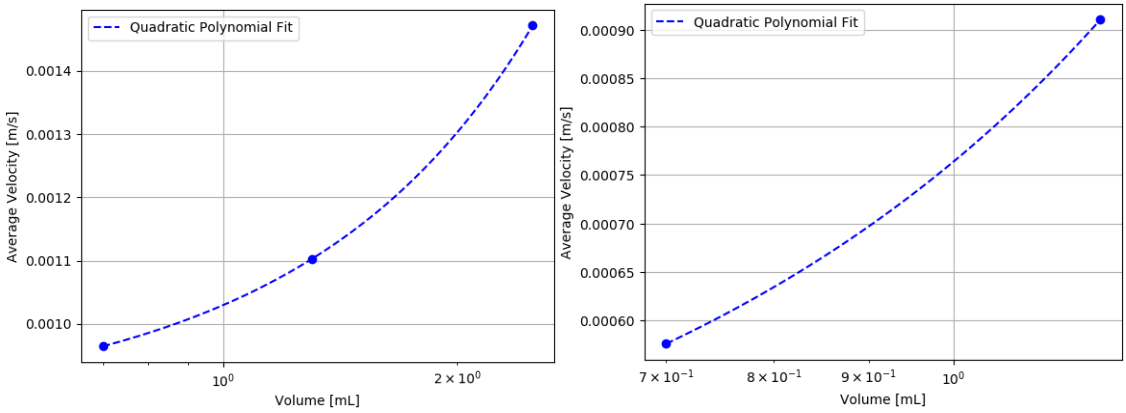

Figure 4: (left) Average velocity of flow in a straight channel compared to volume. (right) Average velocity of flow in channels with gradual and abrupt transitions in width.

Transition	*Relative Position*	*Mean Velocity (m/s)*	*Standard Deviation (%)*
Abrupt	Before	0.00034	± 48
	After	0.00048	± 80
% Increase		71%	
Gradual	Before	0.00077	± 58
	After	0.0018	± 57
% Increase		230%	

Table 3: Velocity changes between gradual and abrupt transitions while comparing the relative position of the fluid.

	Time Elapsed	*Measurement*	*Volume*
Error	$\pm 0.1ms$	$\pm 1\mu m$	$\pm 0.1mL$

Table 4: Reading Errors associated with the error analysis and standard deviations presented.

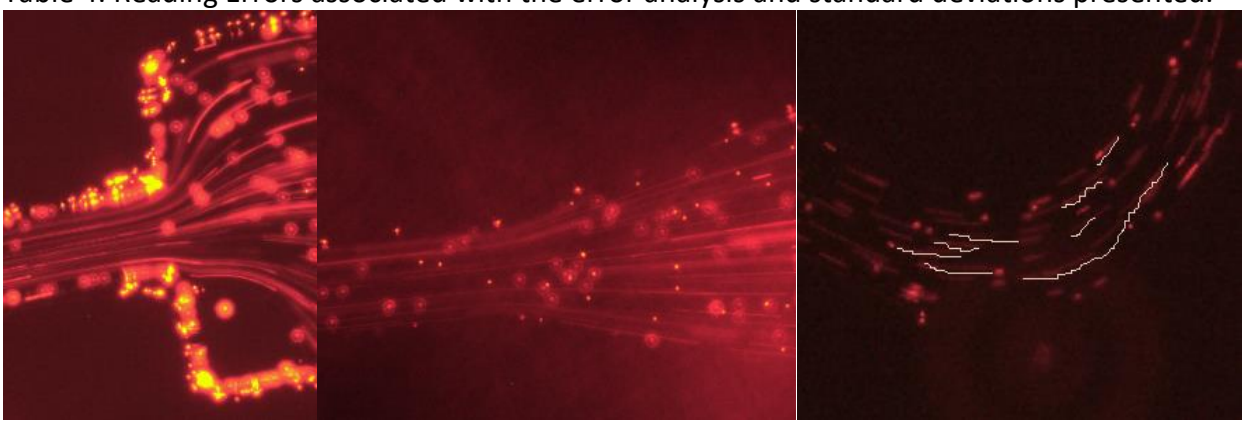

Figure 5: (left) Fluid flow in channel 1 through an abrupt change in width. (middle) Fluid flow in channel 2 with a gradual change in width. (right) Outlined flow of particles through a bend.

Bend	*Relative Position*	*Mean Velocity (m/s)*	*Standard Deviation (%)*
Sharp Turn	Before	0.00090	44
	In Bend	0.0011	45
	After	0.00094	30
Smooth Curve	Before	0.00014	41
	In Bend	0.00022	72
	After	0.00018	73

Table 5: Mean velocity values of the flow before, in, and after a bend categorized by sharp turns (channel 3) and smooth bends (channel 5).